A Novel Communication Paradigm for High Capacity and Security via Programmable Indoor Wireless Environments in Next Generation Wireless Systems

Christos Liaskos[a,*], Shuai Nie[b], Ageliki Tsioliaridou[a], Andreas Pitsillides[c], Sotiris Ioannidis[a], Ian Akyildiz[b,c]

[a] *Foundation for Research and Technology - Hellas (FORTH)*
[b] *Georgia Institute of Technology, School of Electrical and Computer Engineering*
[c] *University of Cyprus, Computer Science Department*

Abstract

Wireless communication environments comprise passive objects that cause performance degradation and eavesdropping concerns due to anomalous scattering. This paper proposes a new paradigm, where scattering becomes software-defined and, subsequently, optimizable across wide frequency ranges. Through the proposed programmable wireless environments, the path loss, multi-path fading and interference effects can be controlled and mitigated. Moreover, the eavesdropping can be prevented via novel physical layer security capabilites. The core technology of this new paradigm is the concept of metasurfaces, which are planar intelligent structures whose effects on impinging electromagnetic waves are fully defined by their micro-structure. Their control over impinging waves has been demonstrated to span from 1 GHz to 10 THz. This paper contributes the software-programmable wireless environment, consisting of several HyperSurface tiles (programmable metasurfaces) controlled by a central server. HyperSurfaces are a novel class of metasurfaces whose structure and, hence, electromagnetic behavior can be altered and controlled via a software interface. Multiple networked tiles coat indoor objects, allowing fine-grained, customizable reflection, absorption or polarization overall. A central server calculates and deploys the optimal electromagnetic interaction per tile, to the benefit of communicating devices. Realistic simulations using full 3D ray-tracing demonstrate the groundbreaking performance and security potential of the proposed approach in 2.4 GHz and 60 GHz frequencies.

Keywords: Wireless, performance, Physical Layer Security, Controlled Propagation, Metasurfaces, Intelligent Surfaces, Millimeter wave.

*Corresponding author
Email addresses: cliaskos@ics.forth.gr (Christos Liaskos), shuainie@ece.gatech.edu (Shuai Nie), atsiolia@ics.forth.gr (Ageliki Tsioliaridou), andreas.pitsillides@ucy.ac.cy (Andreas Pitsillides), sotiris@ics.forth.gr (Sotiris Ioannidis), ian@ece.gatech.edu (Ian Akyildiz)

1. Introduction

Recent years have witnessed a tremendous increase in the efficiency of wireless communications. Multiple techniques have been developed to tackle the stochastic nature of the wireless channel, in an effort to fully adapt to its wide fluctuations. Indoor environments have attracted special attention, since performance and security issues accentuate due to the presence of multiple scatterers in a confined space. In such cases, techniques such as MIMO, beamforming, adaptive modulation and encoding have enabled wireless devices to rapidly adapt to the time-variant, unpredictable channel state [1]. The present work opens an unexplored research path: making the wireless environment fully controllable via software, enabling the optimization of major propagation factors between wireless devices. Thus, effects such as path loss, multi-path fading and interference become controllable, allowing for novel capabilities in performance and physical-layer security.

In order to understand the potential of exerting control over an environment, we first need to define its composition and its natural behavior. Indoor environments, which constitute the focus of the present work, comprise two or more communicating devices–such as laptops, mobile phones, access points, base stations etc.–and any object found in a domestic or work space that can influence their communication. At lower frequencies, walls, ceilings, floors, doors and sizable furniture act as electromagnetic (EM) wave scatterers, creating multiple paths between communicating end-points, especially in non-line-of-sight (NLOS) areas. At higher frequencies, such as millimeter wave (mm-wave) or terahertz (THz), which are expected to play a major role in upcoming 5G communications [2], even small objects act as substantial scatterers. Furthermore, ultra-small wavelengths translate to considerable Doppler shift even at pedestrian speed [2]. These factors, coupled with the natural ambient dissipation of power due to free space losses, lead to undermined NLOS performance at $2-5\,GHz$ and inability for NLOS communications at $60\,GHz$ and beyond [2]. Moreover, transmitted waves cannot be deterministically prevented from reaching unintended recipients, causing interference and allowing for eavesdropping.

Existing proposals for physical-layer performance and security can be classified as i) device-oriented, and ii) retransmitter-oriented. Device-oriented methods include massive MIMO deployments in communicating devices, to make constructive use of the multi-path phenomena [3]. Additionally, beamforming seeks to adaptively align the direction of wireless transmissions in order to avoid redundant free space losses, as well as to spatially contain interference and eavesdropping potential [4, 5]. Additional schemes include the on-the-fly selection of the modulation and encoding scheme that offers the best bit error rate (BER) under the current channel conditions [6]. Retransmission-oriented solutions advocate for the placement of amplifiers in key-positions within the indoor environment. Retransmitters can be either passive or active: Passive retransmitters are essentially conductive structures akin to antenna plates [7].

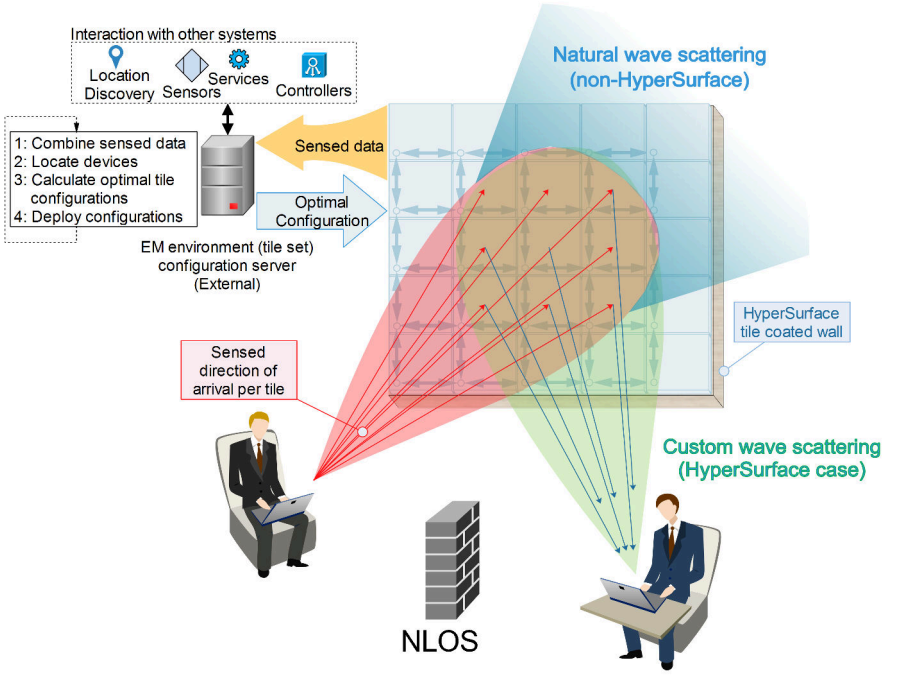

Figure 1: The proposed workflow involving HyperSurface tile-coated environmental objects. The EM scattering is tailored to the needs of the communication link under optimization. Unnatural EM scattering, such as lens-like EM focus and negative reflection angles can be employed to mitigate path loss and multi-path phenomena, especially in challenging NLOS cases.

They passively reflect energy from and towards fixed directions, without tunability. Active retransmitters are powered electronic devices that amplify and re-transmit received signals within a given frequency band. Essentially, they attempt to combat power loss by diffusing more power within the environment. In mm-wave frequencies and beyond, retransmitters must be placed in line-of-sight (LOS) among each other, in an effort to eliminate NLOS areas within a floor plan. Device-to-device networking can also act as a retransmission solution for specific protocols and a limited capacity of served users [8]. The overviewed solutions have a common trait: They constitute device-side approaches, which treat the environment as an uncontrollable factor that does not participate into the communication process. Metasurfaces are the core technology for introducing programmatically controlled wireless environments [9, 10, 11]. They constitute the outcome of a research direction in Physics interested in creating (rather than searching for) materials with required EM properties. In their earlier iterations, they comprised a metallic pattern, called *meta-atom*, periodically repeated over a Silicon substrate, as shown in Fig. 2. The macroscopic EM behavior of a metasurface is fully defined by the meta-atom form. A certain pattern may

fully absorb all impinging EM waves from a given direction of arrival (DoA), while another may fully reflect a given DoA towards another, at a negative reflection angle. Notably, metasurfaces (and their 3D counterpart, the metamaterials) offer a superset of EM behaviors with regard to regular materials. Lens functionality (concentration of reflections towards a given point rather than ambient dispersal) and negative refraction/reflection indices are some of the exotic EM capabilities they can exhibit [12]. Dynamic meta-atom designs allow for dynamic metasurfaces, as shown in Fig. 2. Such designs include tunable factors, such as CMOS switches, microfluidic switches or Micro Electro-Mechanical Switches (MEMS) that can alter their state–and the EM behavior of the metasurface–via an external bias [12]. The bias is commonly electronic, but thermal, light-based and mechanical approaches have been studied as well [12]. Thus, multi-functional metasurfaces, that can switch from one EM behavior to another (e.g., from absorbing to custom steering) are enabled. Finally, a very strong trait is that there is no known limitation to the operating metasurface frequency, which can be at the mm-wave and THz bands [13].

The methodology proposed by the present study is to coat objects of EM significance within an indoor environment with a novel class of software-controlled metasurfaces. The study defines a unit of this metasurface class, called *HyperSurface tile*. A HyperSurface tile is a planar, intelligent structure that incorporates networked hardware control elements and adaptive meta-atom metasurfaces. Following a well-defined programming interface, a tile can receive external commands and set the states of its control elements to match the intended EM behavior. The tiles, covering walls, doors, offices, etc., form networks to facilitate the relaying of programmatic commands among them. Moreover, tiles can have environmental sensing and reporting capabilities, facilitating the discovery of communicating devices within the environment. As shown in Fig. 1, a central server can receive incoming tile reports, calculate the optimal configuration per tile, and set the environment in the intended state by sending the corresponding commands. Collaboration with existing systems (e.g., localization services and loud computing) constitutes a strong aspect of the proposed approach, given that it enables the incorporation of the EM behavior of materials in smart control loops.

The present study contributes the first model to describe programmable wireless indoor environments, detailing their hardware, networking and software components. The model includes the way for translating EM metasurface functionalities to reusable software functions, bridging physics and informatics. Moreover, the protocol specifications and programming interfaces for interacting with tiles for communication purposes are outlined. The practical procedure for deploying and configuring programmable EM environments to mm-wave indoor communication is detailed. The potential of programmable environments is evaluated via full 3D ray tracing in 2.4 and $60\,GHz$ cases, demonstrating their ground-breaking potential in wireless performance and security.

The remainder of the text is organized as follows. Related studies on physical-layer wireless performance and security are overviewed in Section 2. Prerequisite knowledge on metasurfaces is given in Section 3. The HyperSurface-based wire-

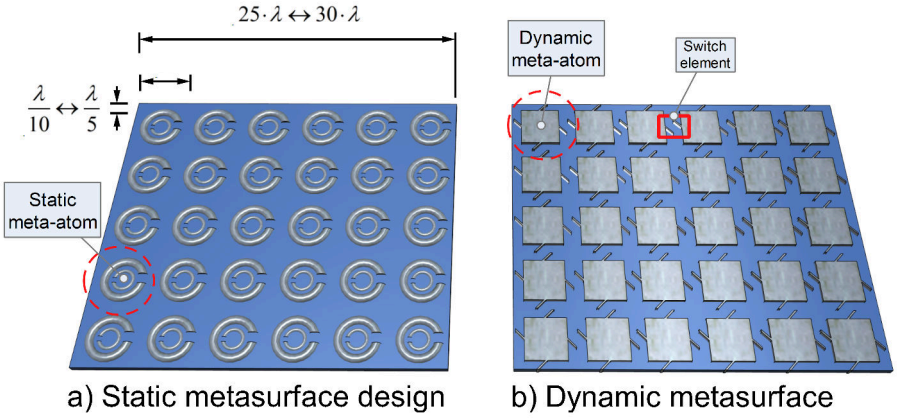

Figure 2: Split ring resonators (left) constituted a very common type of static metasurfaces, with fixed EM behavior. Novel designs (right) incorporate switch elements (MEMS, CMOS or other) to offer dynamically tunable EM behavior.

less environment model is given in Section 4 and its configuration is formulated in Section 5. Applications to indoor wireless setups are discussed in Section 6. Evaluation via ray-tracing-based simulations is presented in Section 7. Finally, the conclusion is given in Section 8.

2. Related Work

Related to programmable wireless environments are the *probabilistic channel control* and *physical layer security* concepts, surveyed in the ensuing subsections.

2.1. Probabilistic Channel Control

The probabilistic channel control describes an approach to influence the behavior of a communications channel not from its end-points (transmitter-receiver), but rather from intermediate points. This has been exhibited with the use of passive objects, phased array antenna panels and un-phased antennas.

The position of passive objects naturally changes the propagation of EM waves within a space. Spaces, such as floorplans, can even be designed and built with EM wireless coverage considerations [14]. In existing spaces, metallic reflectors have been added as means of naturally redirecting EM waves towards areas with poor coverage [7]. This approach does not offer adaptivity or precise control over EM propagation. Moreover, the control type is limited to reflecting EM waves to a natural direction. However, it is simple to deploy and maintain in practice and cost-effective.

Phased array antennas have been used to actively and potentially adaptively alter the probabilistic behavior of a channel. Array panels hung from

Table 1: Comparison of EM wave control techniques.

	Far EM Field Control Type	Near EM Field Control Type	Spatial EM Control Granularity	Hardware Complexity	Deployment Scalability
Phased Array Antennas	Deterministic	Probabilistic	Medium	Highest	Lowest
Un-phased Antennas	Probabilistic	Probabilistic	Low	Low	High
Passive Reflectors	Probabilistic	Probabilistic	None	Lowest	Highest
HyperSurfaces	Deterministic	Deterministic	Highest	Low	High

walls have been shown to influence considerably the communication quality of wireless devices [4, 5]. Phased array antennas comprise several half- or quarter-wavelength antennas, combined with hardware to control their relative phase. Altering the relative phase of an antenna corresponds to a local change in the reflective index of the array [15]. Thus, proper phase configurations allow for anomalous wave steering and even absorbing. However, the phase-based operation is coherent and deterministic only at the far-field. For a square panel with size $D = 0.5$ m and operating frequency of 5 GHz, the far field extends beyond $2(\sqrt{2}\cdot D)^2/\lambda = 16.67$ m. For 60 GHz the far field limit is at 200 m. This constitutes indoors applicability difficult, even for very small panels. Size-able deployments can also be limited by the cost and power consumption of the phase control hardware.

Un-phased antenna deployments have also been proposed as a cheaper and simpler alternative. In this case, simple antennas are placed over planar objects at relatively large distances to avoid coupling effects. Control over the EM waves is exert only at the antenna positions, while most of the surface of the planar object continues to interact uncontrollably with EM waves. Thus, deterministic control is not attained, even at the far-field. Instead, this approach attains a probabilistic effect in the channel behavior, which can be quantified via measurements after deployment has taken place [16].

In differentiation, the present work proposes environments with software-defined, *deterministic wireless propagation*. This is attained by using software-defined metasurfaces as the EM wave control agent [17]. As detailed in Section 3, metasurfaces comprise strongly coupled radiating elements sized at even less than $\lambda/10$. This high resolution of elements has been shown to allow for the micromanagement of EM waves at the level of electric and magnetic field vectors, with state-of-the-art spatial resolution and near unitary efficiency [18]. This enables any kind of custom EM interaction, at any distance from the surface, alleviating the deployment scalability concerns of phased arrays. Moreover, their internal structure is simple: local refractive/reflective index changes over the surface can be attained by simple ON/OFF switches. This simplicity can enable cheap massive production, e.g., as printed structures on films.

The supported features of the related approaches are summarized in Table 1.

2.2. Physical Layer Security

With the pervasive usage of smart wireless devices, security issues have risen to become one of the most concerning aspects among end-users, service

Table 2: Comparison of Physical Layer Security Techniques.

	HyperSurface	Millimeter-Wave Communications	Massive MIMO Communications	Channel Coding	Heterogeneous Networks
Key Techniques	Deterministic Control of EM propagation	Directional Beamforming	Time Division Duplex	LDPC, Polar Codes, Lattice Codes	User Association Policies, Authentication and Authorization
Computation Complexity	Low	High	High	High	High

providers, and policy makers worldwide. Information containing personal credentials or with high security levels should be transmitted and received in reliable channels against adversaries. To combat the attacks of jamming and eavesdropping, traditional security techniques are mostly deployed in the upper layers of the wireless networks, for example, the Wi-Fi Protected Access (WPA) and WPA2 protocols in IEEE 802.11 standards. In a modern cyber-physical system, security methods are also being explored and implemented in the physical layer where signal processing techniques and coding schemes are enhanced for secrecy. In this Section, we briefly survey the state-of-the-art in physical layer security techniques and make a brief comparison and contrast with the HyperSurfaces, in terms of key enabling techniques as well as computation complexity, as shown in Table 2.

Major directions to achieve physical layer security (PLS) include using highly directional antennas to nullify malicious attacks, forming exclusion areas, assigning secret keys to legitimate users, and so on. From the perspective of fundamental propagation channels, the principle of a good secrecy can be achieved is when the eavesdroppers do not have the knowledge of the frequencies where packages are transmitted, or the eavesdroppers are in the same frequency channel but with much higher noise which make the intercepted data impossible to decode [19]. By understanding the attack patterns and corresponding combating strategies, the secrecy capacity can be thus maximized in the wiretap channel [20].

Physical Layer Security on Millimeter-wave Communications

Currently, several millimeter wave (mm-wave) frequency bands (30–300 GHz) are deployed for the next generation wireless communication systems [21]. With the advantage of more available spectrum resources, mm-wave systems can achieve higher throughput compared to lower frequencies. However, the limitation of higher path loss at mm-wave frequencies requires the utilization of highly directional antennas or antenna arrays for communication links to combat noise over a short distance. The characteristics of high directivity and short-range communication are beneficial for link security.

Recent studies have demonstrated that the security performance of a mm-wave communication system relies on the antenna array patterns and the density of eavesdroppers, and by introducing artificial noise to the mm-wave system, the secrecy performance is significantly improved [22, 23, 24]. However, challenges in fully utilizing mm-wave for the purpose of PLS still remain. First, a comprehensive knowledge about mm-wave channel is required for channel estimation, especially the peculiar effects in blockage, atmospheric attenuation, and water

vapor absorption. Second, the computation efficiency in mm-wave beamforming needs to be optimized under the scenario with multiple malicious attacks in a small area.

Physical Layer Security on Massive MIMO Communications

The massive MIMO communication system has the advantage of using very large antenna arrays (with more than one hundred antenna elements) at the transceivers to transmit or receive multiple streams of data simultaneously. In terms of physical layer security, massive MIMO system offers both benefits and drawbacks. On the positive side, the channel condition is stable and easy to predict, which leads to a reduced cost in channel estimation for users. Also, less complicated signal processing burden is brought to both base stations (BSs) and users. However, for eavesdroppers who are actively jamming the channels, these advantages can also serve to their favors, which are the downside of massive MIMO system that needs to be tackled [25].

In order to achieve a desired secrecy level in massive MIMO communications, one important step is to detect malicious activities. The active attacks may forge themselves to act as legitimate users and hence intercept the data from the base station. To solve this problem, several detection strategies are discussed in [26, 27, 28]. For the eavesdroppers who are passively listening to the channel, massive MIMO systems demonstrate good secrecy capacity by power allocation scheme and artificial noise generation [29].

Physical Layer Security on Heterogeneous Networks

The architecture of heterogeneous networks (HetNets) allows for multiple layers of cellular networks to operate with different coverage ranges, transmit powers, radio access schemes, and so on. The extra degrees of freedom in network configurations bring both opportunities and challenges for physical layer security. On one hand, the network configurations for high-power nodes and low-power nodes can be flexible and scalable to account for different channel dynamics, including density of eavesdroppers, mobility of authorized users, and channel fading, just to name a few [24]. On the other hand, the randomness in the HetNet brings the challenges in authorized user association. For example, if a legitimate user only selects the base station with the strongest power, it is also easy for the eavesdroppers to intercept the information. Hence, a trade-off between link session connectivity and security requires the design of user association schemes that also improve secrecy performance.

Additionally, with the burgeoning applications of wireless payment and ad-hoc data exchange, device-to-device (D2D) communications in very short distance among several users requires authentication and authorization strategies to be carefully designed to avoid data leakage to eavesdropping threats. Moreover, the D2D data relaying needs higher security performance and reliable routing schemes to avoid data interception and jamming [30]. The computation complexity for configuring an optimal route with high secrecy capacity will increase as the number of relay nodes increases between two end devices.

Physical Layer Security Coding

Coding schemes play a crucial role in improving a wireless system's physical layer security. Existing codes for secrecy have been discussed and surveyed extensively, which include low-density parity-check codes, polar codes, lattice codes, among many others [31, 32]. The secrecy performance of different codes varies with different channel conditions and types of eavesdropping behaviors. Therefore, challenges still remain as in how to design codes that can maintain desirable level of secrecy in more generalized channel and how coding schemes can be synergistically combined with aforementioned techniques to reach optimal results in future wireless systems.

3. Prerequisites on Metasurfaces

This section provides the necessary background knowledge on metasurfaces, discussing dimensions and composition, operating principles and supported functionalities. The following concise description targets a wireless communications audience, given the topic of the present paper. A more detailed introduction can be found in [18].

A metasurface is a planar, artificial structure which comprises a repeated element, the meta-atom, over a substrate. In most usual compositions, the meta-atom is conductive and the substrate is dielectric. Common choices are copper over silicon, while silver and gold constitute other exemplary conductors [9]. More exotic approaches employ graphene, in order to interact with THz-modulated waves [13]. Metasurfaces are able to control EM waves impinging on them, in a frequency span that depends on the overall dimensions. The size of the meta-atom is much smaller than the intended interaction wavelength, λ, with $\lambda/10 - \lambda/5$ constituting common choices. The thickness of the metasurface is also smaller than the interaction wavelength, ranging between $\lambda/10$ and $\lambda/5$ as a rule of a thumb. Metasurfaces usually comprise a dense population of meta-atoms per area unit, which results into fine-grained control over the EM interaction control. In general, a minimum size of approximately 30×30 meta-atoms is required to yield an intended EM interaction [12].

Figure 2-a illustrates a well-studied metasurface design comprising split-ring resonators as the meta-atom pattern. Such classic designs that rely on a static meta-atom, naturally yield a static interaction with EM waves. The need for dynamic alteration of the EM wave control type has given rise to dynamic metasurfaces, illustrated in Fig. 2-b. Dynamic meta-atoms incorporate phase switching components, such as MEMS, CMOS transistors or microfluidic switches, which can alter the structure of the meta-atom. Thus, dynamic meta-atoms allow for time-variant EM interaction, while meta-atom alterations may give rise to multi-frequency operation [9]. Phase switching components can also be classified into state-preserving or not. For instance, mechanical or microfluidic switches may retain their state and require powering only for state transitions, while semiconductor switches require power to maintain their state.

The operating principle of metasurfaces is given in Fig. 3. The meta-atoms, and their interconnected switch elements in the dynamic case, act as control

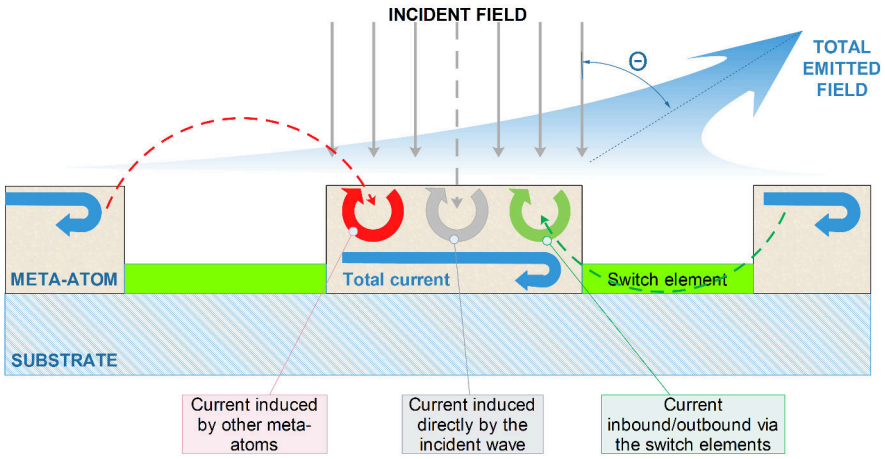

Figure 3: The principle of metasurface functionality. Incident waves create a well-defined EM response to the unit cells. The cell response is crafted in such a way that the aggregate field follows a metasurface-wide design objective, e.g., reflection towards a custom angle Θ.

factors over the surface currents flowing over the metasurface. The total EM response of the metasurface is then derived as the total emitted field by all surface currents, and can take completely engineered forms, such as the unnatural reflection angle shown in Fig. 3. Engineering the total surface current must account for all the currents over the surface. These include: i) currents directly induced over the metasurface by the incident wave, ii) currents induced in a meta-atom wirelessly by other meta-atoms, and iii) currents flowing inwards or outwards from a meta-atom via the switch elements. A qualitative description of the dynamic metasurface operation can also be given: the meta-atoms can be viewed as either input or output antennas, connected in custom topologies via the switch elements. Impinging waves enter from the input antennas, get routed according to the switch element states, and exit via the output antennas, exemplary achieving customized reflection.

3.1. State-of-the-art potential and manufacturing approaches

Metasurfaces constitute the state of the art in EM control in terms of capabilities and control granularity. A metasurface can support a wide range of EM interactions, denoted as *functions*. Common function types include [10]:

- Redirection (refraction or reflection) of an impinging wave, with a given direction of arrival, towards a completely custom direction. Both the reflection and refraction functions can override the outgoing directions predicted by Snell's law. Reflection and refraction functions will jointly be referred to as wave *steering*.
- Beam splitting, i.e., steering a wave towards multiple custom directions in parallel.

- Wave absorbing, i.e., ensuring minimal reflected and/or refracted power for impinging waves.
- Wave polarizing, i.e., changing the oscillation orientation of the wave's electric and magnetic field.
- Wavefront focus, i.e., acting as lens to focus an EM wave to a given point in the near or far field. Collimation (i.e., the reverse functionality) can also be attained.
- Phase control, i.e., altering the phase of the carrier wave.

Moreover, they can offer additional, advanced functions, such as anisotropic response leading to hyperbolic dispersion relation, giant chirality, arbitrary wavefront shaping and frequency selective filtering [11]. Apart from communications, these traits have been exploited in a variety of applications, e.g., highly efficient energy harvesting photovoltaics, and thermophotovoltaics, ultra-high resolution medical imaging, sensing, quantum optics and military applications [33].

The extended repertoire of EM function types, as well the exquisite degree of granularity in EM behavior control, sets metasurfaces apart from phased antennas and reflectarrays [34, 5], which support coarser EM steering and absorbing at the far field, e.g., for beamforming applications in wireless devices [4]. Notice that highly fine-grained EM control is required in mm-wave setups, due to the extremely small wavelength [2].

Regarding their manufacturing approaches, metasurfaces are commonly produced as conventional printed circuit boards (PCBs) [35]. The PCB approach has the advantage of relying on a mature, commercially accessible manufacturing technology. The PCB production cost is moderate (indicatively, USD 500 per m^2 [36]). However, the PCB technology is originally intended for integrated circuits with far greater complexity than a metasurface. As described in the context of Fig. 2, a metasurface can be a very simple structure, comprising a set of conductive patches, diodes and conductive power/signal lines. Therefore, large area electronics (LAE) can constitute better manufacturing approaches in terms of ultra low production cost [37, 38]. LAE can be manufactured using conductive ink-based printing methods on flexible and transparent polymer films, and incorporate polymer/organic diodes [39]. Films with metasurface patterns and diodes printed on them can then be placed upon common objects (e.g., glass, doors, walls, desks), which may also act as the dielectric substrate for the metasurface. It is theorized that printed electronics will reach the manufacturing cost of regular paper printing [40], which has an indicative cost of USD 1.66 per m^2 [41].

4. The HyperSurface-based Programmable Wireless Environment Model

This section details the HyperSurface tile hardware components, the tile inter-networking and the environment control software. A schematic overview is given in Fig. 4 and is detailed below.

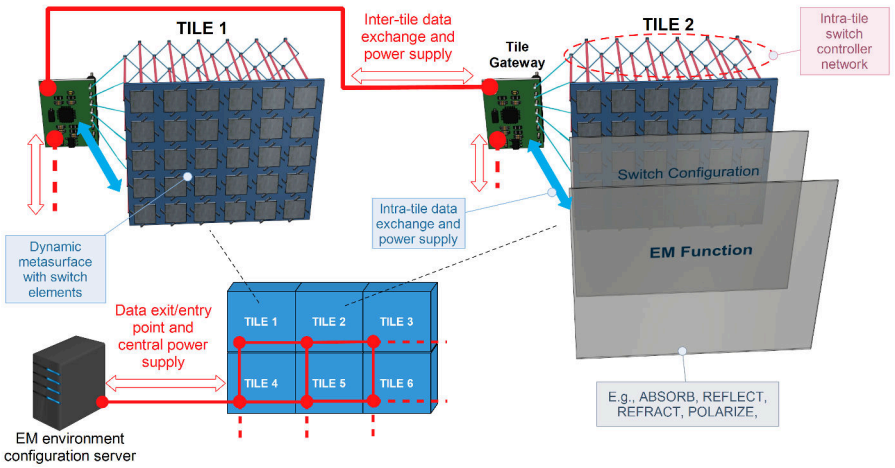

Figure 4: Illustration of the HyperSurface tile architecture and the tile-enabled wireless environment model.

The tile hardware. The tile hardware consists of a dynamic metasurface, a set of networked, miniaturized controllers that control the switch elements of the metasurface, and a gateway that provides inter-tile and external connectivity. The controller network has a slave/master relation to the gateway. Via the gateway, the controller network reports its current state and receives commands to alter the state of the switch elements in a robust manner, making the metasurface yield an overall required EM function.

A single controller is a miniaturized, addressable electronic device that can monitor and modify the state of at least one metasurface switch element. The controller design objectives are small size (to avoid significant interference to the EM function of the metasurface), low-cost (to support massive deployments in many tiles), high monitoring and actuation speed (to sustain fast EM reconfigurability of the metasurface), and the ability to create, receive and relay data packets (to enable controller networking).

The avoidance of EM function disruption also refers to the wiring required to connect the controllers to the switch elements and to each other in a grid topology (cf. Fig. 4). Therefore, the total wiring should also be kept low. The grid-networked controller approach is an option that balances wiring length and robustness to node failures. Bus connectivity for the controllers would minimize the required wiring, but would decrease the robustness against node failures. On the other hand, a star connectivity would offer maximum robustness but would also yield maximum wiring. Notice that future technologies, such as nanonetworking, may enable wireless, computationally-powerful nodes with autonomous, energy harvesting-based power supply [42]. Thus, future tile designs may need no wiring or specific gateways. The setup presented in this study prioritizes cost-effective realizability with present manufacturing capabilities.

At a logical level, a controller is modeled as a finite-state automaton, which reacts to incoming packets or switch element changes by transitioning from one state to another [43]. A UML-standard state diagram should capture three basic controller processes: the data packet handling (including re-routing, consuming packets and sending acknowledgments), the node reporting (reacting to an incoming monitoring directive–monitor request packet–by creating a new monitor data packet), and a fault detection process (either self- or neighbor-failure). The latter is required for robust data routing and for deducing the operational state of the tile as a whole. Regarding the controller addressing, it can be either hardwired– due to the fixed grid topology–or be set dynamically.

The tile gateway stands between the tile controller network and the external world. It is incorporated to the tile fabric at a position selected to yield minimal EM interaction concerns (e.g., at the back of the tile). It provides mainstream protocol-compatible data exchange with any other system. Internally, it is connected to at least one controller, while more connections can be used for robust connectivity. Moreover the gateway acts as a power supply bridge for the tile. Limited size (e.g., $\tilde{}cm$) and energy requirements are the only significant constraints. Existing hardware, such as IoT platforms [44], can be employed as tile gateways [44]. The tile gateway may optionally have EM DoA sensing capabilities, to facilitate the location discovery of wireless user devices in the environment.

Remark 1. It is noted that, in the simplest implementation, the gateway can be directly wired to each metasurface switch, controlling them without the intervention of a controller network. This control approach is similar to LED arrays and monitors, and facilitates the printed film manufacturing approaches described in Section 3.1, which can suffice for programmable wireless environments. The presence of a controller network can enable advanced functions in the future, such as self-maintained intelligent metasurfaces which can sense and alter EM waves autonomously [17].

The tile inter-networking. As tiles are placed over an environmental object, such as a wall, they click together, connecting data and power lines among the tile gateways (cf. Fig. 4). Thus, the tiles form a wired ad hoc network in a grid topology, where existing IoT communication protocols can be readily employed. The same protocol is used for connecting the tile network to any external system. At least one tile–denoted as exit/entry point–has its gateway connected to the environment configuration server, which accumulates sensed data and diffuses EM actuation commands within the tile network. More than one tile can be used as exit/entry points at the same time, for the interest or robust and timely data delivery.

The environment control software. The environment control software is an application programming interface (API) that exists at the configuration server. The API serves as a strong layer of abstraction, hiding the internal complexity of the HyperSurfaces. It offers user-friendly and general purpose access to metasurface functions, without requiring knowledge of the underlying hardware and Physics. It provides software descriptions of metasurface functions, allowing a

programmer to customize, deploy or retract them on-demand over tiles with appropriate callbacks. These callbacks have the following general form:

```
outcome←callback(tile_ID, action_type, parameters)
```

The `tile_ID` is the unique address of the intended tile gateway in the inter-tile network (e.g., an IPv6). One EM function per tile is considered here for simplicity. The `action_type` is an identifier denoting the intended function, such as `STEER` or `ABSORB`, as described in Section 3. Each action type is associated to a set of valid parameters. For instance, `STEER` commands require: i) an incident DoA, $\overrightarrow{I}$, ii) an intended reflection direction, $\overrightarrow{O}$, and iii) the applicable wavelength, λ, (if more than one are supported). `ABSORB` commands require no $\overrightarrow{O}$ parameter. Notice that metasurface properties can be symmetric: i.e., a `STEER` $\left(\overrightarrow{I}, \overrightarrow{O}\right)$ can also result into `STEER` $\left(\overrightarrow{O}, \overrightarrow{I}\right)$ [45].

Once executed at the configuration server, a callback is translated to an appropriate configuration of the switch elements that should be deployed at the intended tile. The configuration is formatted as a data packet that enters the tile network via an entry/exit point, and is routed to the intended tile via the employed intra-tile routing protocol. (An exemplary topology and routing strategy, considering HyperSurface constraints, appears in [46]). The intended tile gateway translates the directive according to the controller network communication protocol specifications and diffuses it within the tile. Upon success, it returns an acknowledgment to the configuration server, or an error notification otherwise.

In the general case, the translation of an EM function to a tile switch element configuration is accomplished via a lookup table, populated during the tile design/manufacturing process as follows. Let σ be a single tile configuration, defined as an array with elements s_{ij} describing the intended switch element state that is overlooked by controller with address i, j in the tile controller network. (One-to-one controller-switch relation is assumed). In the MEMS case, s_{ij} takes binary values, 1 or 0, denoting switch connection or disconnection. Additionally, let Σ be the set of all possible configurations, i.e., $\sigma \in \Sigma$. Let an EM function of type `ABSORB` from DoA $\overrightarrow{I}$ be of interest. Moreover, let $P_\sigma(\phi, \theta)$ be the power reflection pattern of the tile (in spherical coordinates), when a wave with DoA $\overrightarrow{I}$ impinges upon it and a configuration σ is active. Then, the configuration σ_{best} that best matches the intended function `ABSORB` $\left(\overrightarrow{I}\right)$ is defined as:

$$\sigma_{best} \leftarrow argmin_{\sigma \in \Sigma} \left\{ max_{\forall \phi, \theta} P_\sigma(\phi, \theta) \right\} \tag{1}$$

Existing heuristic optimization processes can solve this optimization problem for all functions of interest in an offline manner [47], using simulations or field measurements on prototypes. The configuration lookup table is thus populated. Finally, we note that analytical results for the EM function-configuration relation exist in the literature for several metasurface designs [47]. In such cases, the analytical results can be employed directly, without the need for lookup tables.

5. Controlling Programmable Wireless Environments

In this Section we formulate the problem of optimally configuring a programmable wireless environment to serve performance and security objectives. The formulation is intended to facilitate the creation of automatic environment configuration algorithms, as exemplary shown later in Section 7.

5.1. Wireless Performance Objectives

In order to establish communication links between transmitters and receivers, the HyperSurface tiles need to be adaptively selected and optimally controlled to serve the desired receivers. Since in real-world communication scenarios, multiple users can be present in the same space, it is necessary to discuss the tile distribution and control algorithms.

We start from the case where there is one pair of transmitter and receiver in the environment, as shown in Fig. 6. When the transmitter sends signals, multiple tiles can sense the transmitted signals [48]. According to the location of the receiver sensed by the location discovery system, those tiles will steer their angles to establish reflection paths. Therefore, the signal received at the receiver is a superposition of all signals reflected from various tiles. In the particular case of Fig. 6, among all tiles, only those that can sense the transmitted signals need to respond to forwarding requests and tune their angles. On the other hand, in a more complicated case where multiple users are present in the same environment, the tile distribution needs to be optimized. The signals to be received by different users should be orthogonal to each other and are forwarded by different HyperSurface paths.

We assume the transmitted signal is QPSK modulated with symbol $k(t)$, thus in general the received signal in time domain can be expressed as

$$r(t) = k(t) \sum_{i=1}^{N} a_i e^{-j\theta_i} e^{j2\pi f_c \tau_i} + n(t), \tag{2}$$

where f_c is the central frequency, a_i, θ_i, and τ_i are the attenuation, phase, and delay caused by the reflection paths along HyperSurface tiles of i-th path, and $n(t)$ is the AWGN noise in the channel. We assume there are in total N paths found between the transmitter and receiver. The multipath effects might cause distortion in overall received signal, therefore we need to mitigate the destructive interference and harmonize the phases by controlling the operation of HyperSurface tiles. Specifically, we can formulate it as an optimization problem aimed at maximizing the received power, $P_r^{(j)}$, and the number of tiles of the HyperSurface, $M_{HS}^{(j)}$, for the j^{th} receiver in the network with a total of J users

with d_j distance, as follows:

$$\textit{Given:} (x_t, y_t, z_t), (x_r^{(j)}, y_r^{(j)}, z_r^{(j)}), \tag{3}$$

$$P_t^{\text{total}}, M_{HS}^{\text{total}} \tag{4}$$

$$\textit{Find: } P_t^{(j)}, M_{HS}^{(j)} \tag{5}$$

$$\textit{Objective: } \max \sum d_j P_r^{(j)} \tag{6}$$

$$\textit{Subject to:}$$

$$\text{Transmit power allocation: } \sum P_t^{(j)} \leq P_t^{\text{total}} \tag{7}$$

$$\text{HyperSurface tile allocation: } \sum M_{HS}^{(j)} \leq M_{HS}^{\text{total}} \tag{8}$$

$$\text{for all } j \in J \tag{9}$$

In the above optimization problem, (x_t, y_t, z_t) and $(x_r^{(j)}, y_r^{(j)}, z_r^{(j)})$ denote the three-dimensional coordinates of the transmitter and the i^{th} receiver, respectively. Based on the above optimization problem, we can distribute tiles to corresponding users without causing interference or signal distortion.

5.2. Physical-Layer Security Objectives

We proceed to study two approaches for advanced physical layer security in programmable wireless networks.

Approach 1. The first approach requires the deployment of air-paths that cause zero or trivial interference to unintended users, naturally blocking eavesdropping. The differentiation from the performance objective is that the selection of air-paths prioritizes minimal interference to unintended users, rather than maximal received power to the intended. This can lead to improbable air-paths, e.g., long paths going around crowded places, or paths confined above a given height within a floorplan. We formulate this approach as follows:

$$\textit{Given: } (x_t, y_t, z_t), \tag{10}$$

$$(x_r^{(i)}, y_r^{(i)}, z_r^{(i)}), \tag{11}$$

$$(x_r^{(u)}, y_r^{(u)}, z_r^{(u)}), \tag{12}$$

$$P_{tx}^{\text{tot}}, N_r^{\text{tot}}, N_t^{\text{tot}}, \vec{n}_t^{initial} \tag{13}$$

$$\textit{Find: } N_t, \vec{n}_t^{(s)} \tag{14}$$

$$\textit{Objective: } \min P_r^{(i,u)}, \max P_r^{(i,i)} \tag{15}$$

$$\textit{Subject to:}$$

$$\text{Transmit power allocation: } \sum P_t^{(i)} \leq P_{tx}^{\text{tot}} \tag{16}$$

$$\text{HyperSurface tiles allocation: } N_t \leq N_t^{\text{tot}} \tag{17}$$

In the above optimization problem, parameters (x_t, y_t, z_t), $(x_r^{(i)}, y_r^{(i)}, z_r^{(i)})$, and $(x_r^{(u)}, y_r^{(u)}, z_r^{(u)})$ denote the three-dimensional coordinates of the transmitter, the intended receiver, and unintended receivers, respectively. The total

number of receivers in the environment is denoted as N_r^{tot}. The initial condition of HyperSurface tiles are also known, which is denoted as $\vec{n}_t^{initial}$. In order to minimize the received power of unintended users trying to overhear $P_r^{(i,u)}$ while maximizing the intended user's power $P_r^{(i,i)}$, we need to find the number of tiles N_t and adjust the tiles' orientation to the correct angles, i.e., deploy a proper steering functionality. In terms of formulation this can be seen as finding the normal vectors of the selected tiles $\vec{n}_t^{(s)}$. The resources include the transmit power that is upper-bounded by P_{tx}^{tot}, the number of HyperSurface tiles that are selected N_t which is bounded by the total number of tiles stays below N_t^{tot}.

Approach 2. It is possible that a floorplan does not offer air-paths that avoid other users completely. To address this case, approach 2 seeks to "scramble" the reflected paths along propagation, while still able to recover the original paths at the final bounces. This can be done by altering the phases of the multipaths which belong to the same cluster to achieve coherence, thus the signals' magnitude can still be preserved. Upon the final bounce, the phase difference should be minimized to zero to recover the signals. The objective function is formulated as follows:

$$
\begin{aligned}
\textit{Given: } & (x_t, y_t, z_t), && (18)\\
& (x_r^{(i)}, y_r^{(i)}, z_r^{(i)}), && (19)\\
& (x_r^{(u)}, y_r^{(u)}, z_r^{(u)}), && (20)\\
& P_{tx}^{\text{tot}}, N_r^{\text{tot}}, N_t^{\text{tot}}, \vec{n}_t^{initial} && (21)\\
\textit{Find: } & N_t, \vec{n}_t^{(s)} && (22)\\
\textit{Objective: } & \min P_r^{(i,u)}, && (23)\\
& \max P_r^{(i,i)}, && (24)\\
& \Delta\Phi_n^{(p,q)} = 0 && (25)\\
\textit{Subject to: } & && \\
\text{Phase difference control: } & 0 < \Delta\Phi_j^{(p,q)} \leq \pi/2, && (26)\\
& \text{where } 1 \leq p, q \leq N_{mpc}^{\text{tot}}, && (27)\\
& \text{and } 1 \leq j \leq n-1 && (28)\\
\text{Transmit power allocation: } & \sum P_t^{(i)} \leq P_{tx}^{\text{tot}} && (29)\\
\text{HyperSurface tiles allocation: } & N_t \leq N_t^{\text{tot}} && (30)
\end{aligned}
$$

In the above optimization problem, parameters (x_t, y_t, z_t), $(x_r^{(i)}, y_r^{(i)}, z_r^{(i)})$, and $(x_r^{(u)}, y_r^{(u)}, z_r^{(u)})$ denote the three-dimensional coordinates of the transmitter, the intended receiver, and unintended receivers, respectively. The total number of receivers in the environment is denoted as N_r^{tot}. The initial condition of HyperSurface tiles are also known, which is denoted as $\vec{n}_t^{initial}$. In order to minimize the received power of unintended users trying to overhear $P_r^{(i,u)}$ while maximizing the intended user's power $P_r^{(i,i)}$, we need to find the number

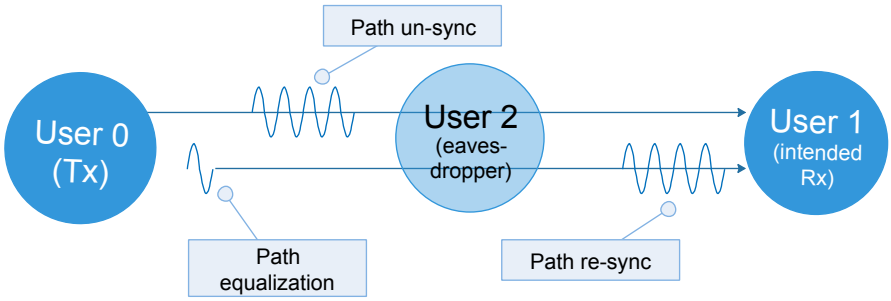

Figure 5: Illustration of the phase control-based approach for eavesdropping mitigation.

of tiles N_t and adjust the tiles' orientation to induce the phase changes $\Delta\Phi_j^{(p,q)}$ among multipaths p, q in the j-th reflection, which corresponds to find the normal vectors of the selected tiles $\vec{n}_t^{(s)}$. The resources include the phase difference controlled by the tiles, the transmit power that is upper-bounded by P_{tx}^{tot}, the number of HyperSurface tiles that are selected N_t which is bounded by the total number of tiles stays below N_t^{tot}.

The phase control-based approach is conceptually illustrated in Fig. 5. We consider two users, a transmitter (user 0) and the intended receiver (user 1), as well as an eavesdropped (user 2) located somewhere between two of the wave propagation paths. The paths are assumed to carry approximately the same end-to-end power. At first, a tile located over the path before the eavesdropper adds an equalization phase to the fastest path, ensuring synchronicity at the user 1. Then, one of the paths is set to negative phase with regard to the other, by using a tile located before user 2. This phase is canceled out by using a tile between user 2 and user 1. In this manner, the eavesdropper sees a total sum of zero received power, while the reception is optimized at the intended user 1.

6. Applications to Mm-wave Indoor Setups

In mm-wave setups, major factors affect the signal attenuation: i) the increased free space path loss (e.g., $\sim 90\,dB$ at $10\,m$ for $60\,GHz$, instead of $60\,dB$ for $2.4\,GHz$), ii) acute multi-path fading even in LOS cases, iii) strong Doppler shift even at pedestrian speeds, and iv) optical-like propagation of EM waves, limiting connectivity to LOS cases and exhibiting strong sensitivity to shadowing phenomena. Attenuation due to molecular absorption may not play a significant role in indoor cases–depending on the composition of the environment–as it corresponds to $10^{-5}\,dB/m$ loss [1].

Given the mentioned mm-wave considerations, we proceed to present mitigation measures offered by a HyperSurface-enabled environment. We consider the setup of Fig. 6, comprising a receiver (Rx)-transmitter (Tx) pair located in NLOS over a known floorplan. The walls are coated with HyperSurface tiles. Furthermore, we consider the existence of a location discovery service

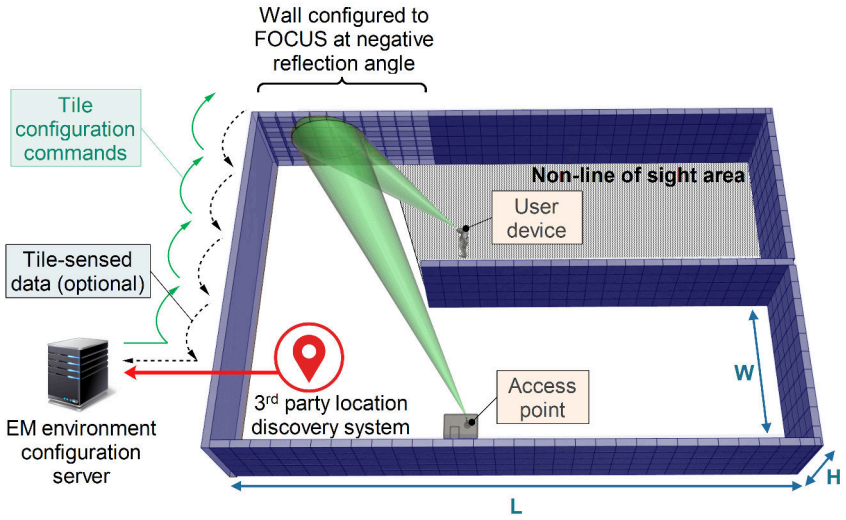

Figure 6: Illustration of a customized wireless indoor environment. `STEER` functions are applied to several tiles, to achieve a `FOCUS` behavior of the corresponding wall as a whole.

(e.g., [49]), which reports the location of the user device. At first, the Rx and Tx may attempt high-power, omni-directional communication. The location discovery service pinpoints the location of the user device and sends it to the EM environment configuration server. (Without loss of generality, the location of the Tx/access point can be considered known). Tiles may sense their impinging power and report it to the server as well. The server can use this information to increase the accuracy of the discovered user device location. Subsequently, the following actions take place:

- The tiles at the top-left part of Fig. 6 are set to a symmetric "negative focus" setup as shown.
- The Tx and the Rx are signaled to direct their antenna patterns to the configured tiles using beamforming.

Unused tiles can be deactivated, reverting to regular, passive propagation. Using this approach, the path loss can be even fully mitigated, since the emitted energy is focused at the communicating end-points, rather than scattering within the environment. This can also be of benefit to the user device's battery lifetime, given that the redundantly emitted power is minimized. Concerning multi-path fading, the fine-grained EM control over the wave propagation can have as an objective the *crafting* of a power delay profile that mitigates the phenomenon, e.g., by ensuring a path with significantly more power than any other, or one that best matches the MIMO capabilities of the devices. Additionally, the focal point of the EM wave reflected by the tiled wall towards the use device can be

altered in real-time, to match the velocity of the mobile user. Mobile trajectory predictions can be employed to facilitate this course of action. This provides a potential mitigation approach for Doppler phenomena.

The environment optimization for multiple user pairs, or sub-spaces within the environment, may be of increased practical interest. Returning to the setup of Fig. 6, the configuration server can, e.g., set the tiles to preemptively minimize the delay spread within the whole NLOS area, while ensuring a minimum level of received power within it. In the sub-space optimization case, the best matching tile configurations can be calculated offline and be deployed upon request. This approach is evaluated in Section 7.

Finally, it is noted that the programmable environment extends the communication distance of devices, without requiring extra dissipation of energy within the environment (e.g. by placing additional access points). This can constitute a considerable advantage for mm-wave communications, which are known to be absorbable by living tissue. Moreover, assuming tiles with state-preserving switch elements, the energy footprint of the programmable environment can be extremely low, especially in static or mildly changing user positions.

7. Evaluation in $60\,GHz$ and $2.4\,GHz$ setups

In this Section we evaluate the performance and security prospects of programmable wireless environments. The evaluation employs full 3D, ray-tracing-based simulations. Different approaches for optimizing the environment are demonstrated per each case.

7.1. Performance objectives

We proceed to evaluate the HyperSurface potential in mitigating the path loss and multi–path fading effects. The indoor 3D space of Fig. 6 is ported to a full-3D ray-tracing engine [50], customized to take into account HyperSurface tile functions. The evaluation focuses on finding tile configurations that optimally mitigate the path loss and multi–path fading for 12 users within the NLOS area. We study the case of $60\,GHz$, which is of increased interest to upcoming 5G communications, as well as the $2.4\,GHz$ case due to its wide applicability, e.g., to WiFi setups [2].

Concerning the simulation parameters, the space has a height of $H = 3\,m$, corridor length (distance between opposite wall faces) $L = 15\,m$, corridor width $W = 4.5\,m$, a middle wall length of $12\,m$, and $0.5\,m$ wall thickness. Two stacked walls exist in the middle. The floor and ceiling are treated as plain, planar surfaces composed of concrete, without HyperSurface functionality. All walls are coated with HyperSurface tiles, which are square-sized with dimensions $1\times1\,m^2$. Thus, the 3D space comprises a total of 222 tiles.

The dynamic metasurface pattern of Fig. 2 is considered using state-preserving switches (e.g., microfluidic). Appropriate dimensions are assumed, for $60\,GHz$ and $2.4\,GHz$ respectively, as explained in the context of Fig. 2. This pattern design has been extensively studied in literature, offering a wide range of

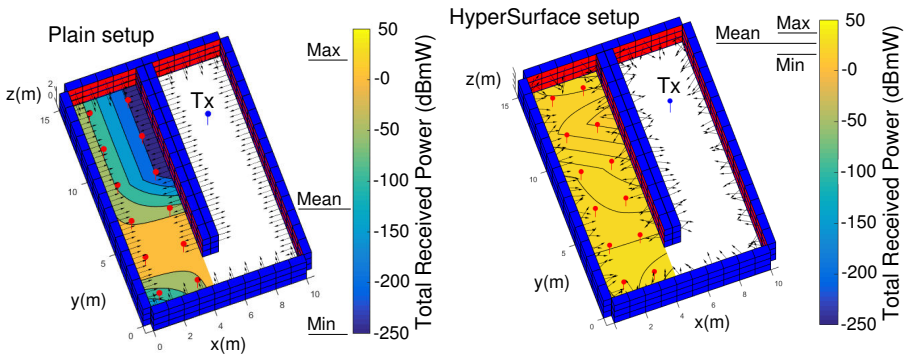

Figure 7: Wireless environment optimization case study (A) for $60\,GHz$ and comparison to the plain case (non-HyperSurface). The objective is to maximize the minimum total received power over the NLOS area receivers (red dots).

steering and absorbing capabilities, even with switch elements only at the horizontal direction [47, p. 235]. Although beyond of the present scope, it is noted that this metasurface design also exhibits tunable EM interaction frequency, yielding a particularly extended repertoire of supported tunability parameters. The considered tile functions account for EM wave steering and absorption from various DoAs. Specifically, we allow for any DoA and reflection direction resulting from the combination of $\{-30^o, -15^o, 0^o, 15^o, 30^o\}$ in azimuth and $\{-30^o, -15^o, 0^o, 15^o, 30^o\}$ in elevation planes, using the tile center as the origin. Notice that the considered angles have been shown to be commonly attainable by metasurfaces [51]. However, carefully designed, static metasurfaces have achieved nearly full angle coverage, i.e., almost $(-90^o, 90^o)$ in azimuth and elevation, which is indicative of their potential [52]. The reflection coefficient is set to 100% for each steering function [47, p. 235]. Additionally, we consider an EM absorbing tile function which reduces the power of impinging waves (given DoA) by $35\,dB$ [47, p. 235], scattering the remaining wave power towards the Snell's law-derived reflection direction. Thus, a tile supports 26 different function configurations in total. Existing ray-tracing engines employ common laws of optics to simulate the propagation of waves. As such, current ray-tracers do not readily allow for custom wave steering functions. (Absorbing functions, on the other hand, are readily supported). Thus, to implement steering functions we work as follows. First, the following observation is made:

Remark 2. Assume a tile and a set of a required wave DoA and a reflection direction upon it, not abiding by Snell's law. There exists a rotation of the tile in 3D space that makes the wave DoA and reflection direction comply with Snell's law.

Based on this Remark, the custom steering functions are implemented by tuning the tile's spatial derivative as follows. Since a tile is a flat and square surface in a 3D space, its spatial derivative is normally an arrow perpendicular

to the tile surface. In order to allow for custom EM wave steering within the ray-tracing engine, we allow for virtually rotating the spatial derivative (but not the tile itself) by proper azimuth and elevation angles. The modified spatial derivative is then used in all ray-tracing calculations.

The external service is considered to know the tile specifications, i.e., the tile configuration that corresponds to each virtual angle combination. The service has obtained the direction of the impinging wave at each tile via the distributed sensing elements. Subsequently, it deploys the corresponding STEER or ABSORB commands at each tile, by applying the corresponding tile configuration.

An EM Tx is placed at position $\{7, 12, 2\}\ m$ (with respect to the origin placed on the floor level, at the upper-left corner of Fig. 6). It is equipped with a half-dipole antenna and transmits at a carrier frequency of $60\,GHz$ or $2.4\,GHz$ (two studies) and $25\,MHz$ bandwidth. The transmission power is set to $100\,dBmW$, a high number chosen to ensure that no propagation paths are disregarded by the ray-tracer due to its internal, minimum-allowed path loss threshold. The NLOS area is defined as $x \in [0, 4]\ m$, $y \in [0, 15]\ m$ and a constant height of $z = 1.5\,m$. Within the NLOS area, a set of 12 receivers–with antennas identical to the transmitter–are placed at a regular 2×6 uniform grid deployment, with $2.5\,m$ spacing. The receiver grid is centered in the NLOS area. Intermediate signal reception values, used only for illustration purposes in the ensuing Figures, are produced by means of interpolation.

The evaluation scenario considers two case studies, corresponding to the path loss and multi-path fading mitigation objectives. In each case, the state of each of the 222 tiles is treated as an input variable of an appropriate objective function which must be optimized. Given the vastness and discontinuity of the solution space (i.e., 222^{26} possible tile configurations, positioned at different walls) and the discrete nature of the input variables, a Genetic Algorithm (GA) is chosen as the optimization heuristic [47], using the MATLAB Optimization Toolbox implementation [53]. GAs are heuristics that are inspired by evolutionary biology principles. They treat the variables of an optimization problem as *genomes* which compete with each other in terms of best fitness to an optimization objective. Good solutions are combined iteratively by exchanging *genes*, i.e., variable sub-parts, producing new generations of solutions. In the problem at hand, a genome represents a complete tile configuration, i.e, an array containing the state of the 222 tiles. A gene represents the state of each tile, i.e., the specific array elements. Two optimization cases are studied, denoted as (A) and (B), both for $60\,GHz$ and $2.4\,GHz$. These are defined as follows:

- **Case study (A)**. This case expresses the path loss mitigation goal, and is defined as the following optimization objective: *Define the optimal tile configurations that maximize the minimum received power over the 12 receivers in the NLOS area.*

- **Case study (B)**. The case expresses the multi-path fading mitigation goal and is defined as the following optimization objective: *Define the optimal tile configurations that minimize the maximum delay spread over the 12*

Table 3: Comparison of total received power (case A) and power delay profile (case B) with and without HyperSurface (HSF) Tiles at $60\,GHz$.

	Case A ($dBmW$)		Case B ($nsec$)	
	HSF setup	Plain setup	HSF setup	Plain setup
Max	34.98	22.63	0.69	3.6
Mean	25.38	-75	0.0068	0.48
Min	16.13	-250	0.0045	0.007

receivers in the NLOS area, with the constraint of ensuring a minimum total received power (custom threshold).

For Case (B), the thresholds are set to $1\,dBmW$ for $60\,GHz$, and $30\,dBmW$ for $2.4\,GHz$, based on the floor-plan dimensions and the path loss levels discussed in Section 6. The results for the $60\,GHz$ case are shown in Fig. 7, 8 and are summarized in Table. 3. Figure 7 presents case (A) for the plain (left) and HyperSurface-enabled (right) environments. In the plain setup, the tile spatial derivatives (black arrows) are naturally perpendicular to the tile surfaces. The average received power over the 12 NLOS area receivers is $-75\,dBmW$, while the minimum power is $-250\,dBmW$, which is the lowest level allowed by the ray-tracing engine. Thus, the bottom-left and the three top-right receivers of the NLOS area are essentially disconnected in the plain setup. The maximum total received power is $22.63\,dBmW$.

The right inset of Fig. 7 shows the corresponding results with the HyperSurface functionality enabled. Notably, the minimum power level over the NLOS area is $16.13\,dB$, which constitutes a raise by at least $266.13\,dBmW$ with regard to the plain case. Moreover, the received power becomes essentially uniform over the NLOS area, ranging between 16.13 and $34.98\,dBmW$, with an average of $25.38\,dBmW$. The tile spatial derivatives exhibit a degree of directivity towards the previously disconnected area parts (e.g., cf. left-most wall). Moreover, the top-and bottom tiles across the height of the walls tend to focus towards the NLOS area height. The non-uniformity of the derivatives is in accordance with the nature of the Genetic Algorithm, which is a very exploratory but not gradient-ascending optimizer [54]. This means that there exists potential for an even better optimization result near the Genetic Algorithm-derived solution. The case (B) results for $60\,GHz$ are shown in Fig. 8. The objective is to minimize the maximum delay spread over the 12 NLOS receivers, under the constraint for at least $1\,dBmW$ total received power per receiver. For the plain setup, shown in the left inset, we note a maximum delay spread of approximately $3.6\,nsec$. The $1\,dBmW$ minimum power constraint is of course not satisfied, as previously shown in Fig. 7-left. The circled areas correspond to the under-powered/disconnected NLOS area parts. The minimum and average delay spread over the *connected* areas only are $7\,psec$ and $0.48\,nsec$ respectively. The HyperSurface-enabled setup (right inset), achieves 5.21 times lower maximum delay spread ($0.69\,nsec$) than the plain setup, a minimum of $4.5\,psec$ delay spread (1.5 times lower), and an average of $6.8\,psec$ (70 times lower). This sig-

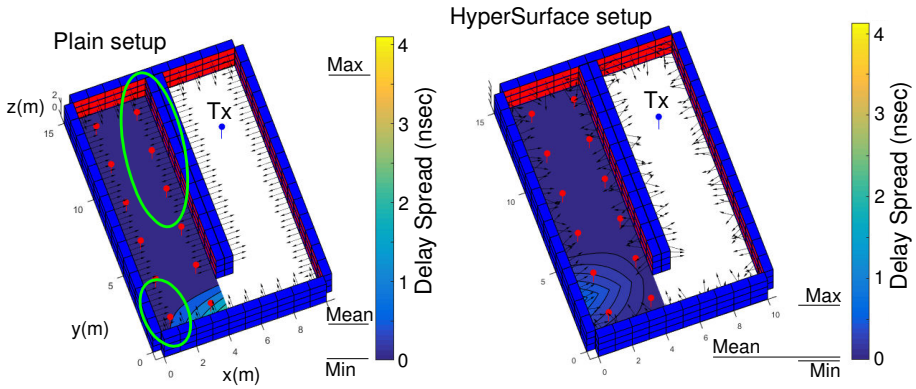

Figure 8: Wireless environment optimization case study (B) for $60\,GHz$. The objective is to minimize the maximum delay spread over the NLOS area, while ensuring a minimum of $1\,dBmW$ total received power per receiver. The circled parts of the plain setup correspond to disconnected areas. (cf. Fig. 7-left).

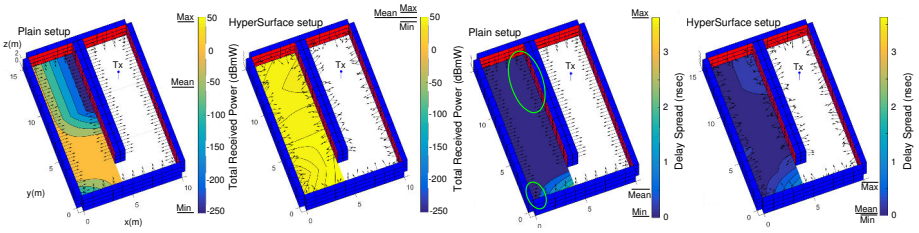

Figure 9: Wireless environment optimization case studies (A: left-two insets) and (B: right-two insets) for the $2.4\,GHz$ case.

nificant performance improvement is accompanied by considerable total power levels, in the range of [7.07, 16.93] $dBmW$ (average: $10.64\,dBmW$), fulfilling the optimization constraint of $1\,dBmW$. The results for the $2.4\,GHz$ case are similar to the $60\,GHz$ in terms of improvement, and are collectively given in Fig. 9 and Table 4. The objective in the two leftmost panels is to maximize the minimum total received power over the 12 receivers in the NLOS area. The plain setup achieves -250, -58 and $47\,dBmW$ minimum, average and maximum total received power, respectively. The HyperSurface setup yields considerably improved results, with 45.13, 51.37 and $59.81\,dBmW$ minimum, average and maximum total received power, respectively. Thus, there is a gain of $295.13\,dBmW$ in minimum received power.

The delay spread improvement is also significant, as shown in the two rightmost panels. The plain setup yields $1.4\,psec$, $0.47\,nsec$ and $3.65\,nsec$ minimum, average and maximum delay spread values, with 4 disconnected receivers (circled parts, cf. first inset of Fig. 9). The corresponding HyperSurface-enabled setup

Table 4: Comparison of total received power (case A) and power delay profile (case B) with and without HyperSurface (HSF) Tiles at $2.4\,GHz$.

	Case A ($dBmW$)		Case B ($nsec$)	
	HSF setup	Plain setup	HSF setup	Plain setup
Max	59.81	47	0.68	3.65
Mean	51.37	−58	0.067	0.47
Min	45.13	−250	0.0029	0.0014

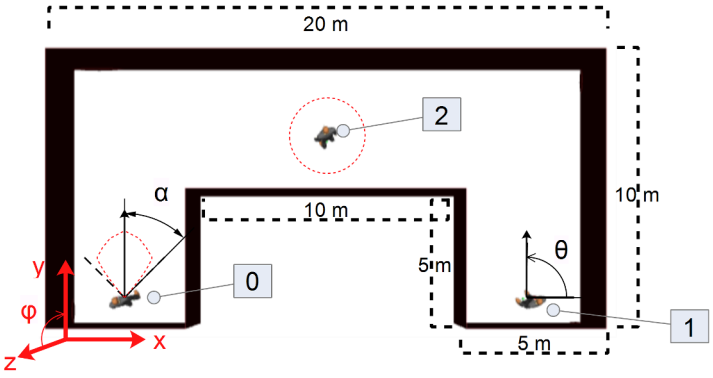

Figure 10: Setup for the eavesdropping mitigation evaluation scenario. User 0 seeks to send data to user 1, and user 2 acts as the eavesdropper.

achieves $2.9\,psec$, $67\,psec$ and $0.68\,nsec$ min/average/max respectively. Moreover, it ensures a minimum total received power of $34.12\,dBmW$, successfully meeting the $30\,dBmW$ optimization constraint.

7.2. Security objectives

We proceed to evaluate the eavesdropping mitigation approaches described in Section 5.2, i.e., avoid an eavesdropper by routing rays away from him, or by tuning the phase of rays in order to cancel each other out near the eavesdropper. To this end, we consider the setup of Fig. 10. Two users, a transmitter (user 0) and a receiver (user 1) are placed in a NLOS setting, with an eavesdropper (user 2) located in-between. Table 5 describes the parameters of the setup. The following notes are made:

- The assumed programmable wireless environment deployment is partial. Only the ceiling and the highest part of the walls are covered with tiles. This approach provides cost and deployment advantages. First, fewer tiles naturally translate to lower cost and overall complexity. Furthermore, ceilings and upper parts of walls are commonly vacant of other use, while offering easy access to power supply (e.g., via the lights power lines).

- The tiles are considered to attenuate impinging waves by a constant factor

Table 5: Simulation parameters / security objectives.

User 0 position	$x: 2.5, y: 1, z: 1\,m$
User 1 position	$x: 17.5, y: 1, z: 1\,m$
User 2 position	$x: 10, y: 7, z: 1\,m$
Ceiling Height	$3\ m$
Tile Dimensions	$75 \times 75\,cm$
Tile Placement	Ceiling, Upper part of walls (> 1.5 m)
Tile Power loss	1 % per ray bounce
Tile Functions	COLLIMATE, STEER, PHASE_ALTER
Frequency	$2.4\,GHz$
Tx Power (User 0)	$-30\,dBm$
Antenna types	Users 0, 1 Single lobe sinusoid ($\alpha = 30^o$)
	User 2 (Eavesdropper) $\rightarrow$isotropic
Antenna orientation	Fig 11, Users 0, 1 : ($\theta = 90^o$, $\phi = 90^o$)
	Fig 12, Users 0, 1 : ($\theta = 90^o$, $\phi = 0^o$)
Max ray bounces	50
Min considered ray power	-250 dBm

of 1 % of the carried power, which constitutes a typical efficiency index for state-of-the-art metasurfaces [18].

- The considered tiles functionalities include collimation and carrier phase control [12]. Collimation is the effect of aligning EM waves to propagate over a flat front, rather than to dissipate over an ever-growing sphere. Thus, the path loss between two tiles is not subject to the $\propto 1/d^2$ rule, d being their distance. This rule is only valid for the first impact, i.e., from the transmitter to its LOS tiles. The antenna aperture and gains are taken into account as usual. The phase control is required only for the corresponding physical later security approach, described in Section 5.2.

- The antenna patterns of the transmitter and the receiver are simplified as single-lobe sinusoids, with the characteristics and θ, ϕ orientiation shown in Fig. 10 and Table 5. In one scenario, we assume that the mobile devices have beamforming capabilites and are able to turn the antenna lobe towards the ceiling, in conjunction with the mobile devices' gyroscopes.

- The eavesdropper's antenna is considered to be isotropic. Moreover, all rays pass through him unobstructed. In contrast, the bodies of the users are modeled as spheres of radius 0.5 m, fully blocking impinging waves.

Figure 11 shows the natural propagation, in an environment without Hyper-Surfaces. The propagation is expectedly chaotic, while several rays are visibly intercepted by the eavesdropper. On the other hand, the propagation in the case of programmable wireless environments is more well-defined, as shown in Fig. 12. In this case, the user devices have employed beamforming to turn their

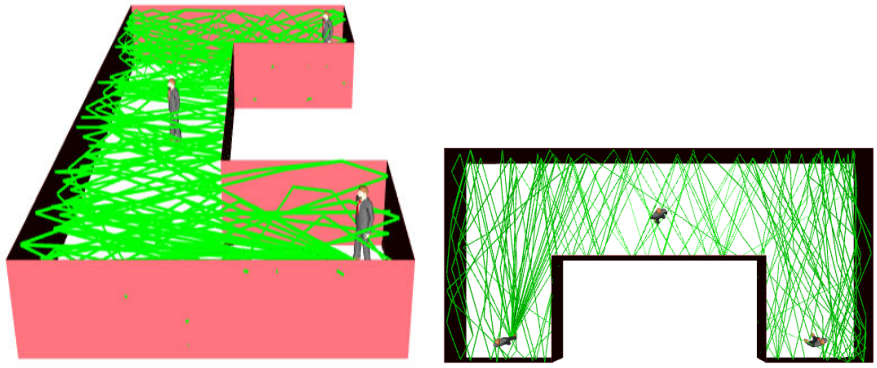

Figure 11: Natural propagation (without HyperSurfaces), side and top views.

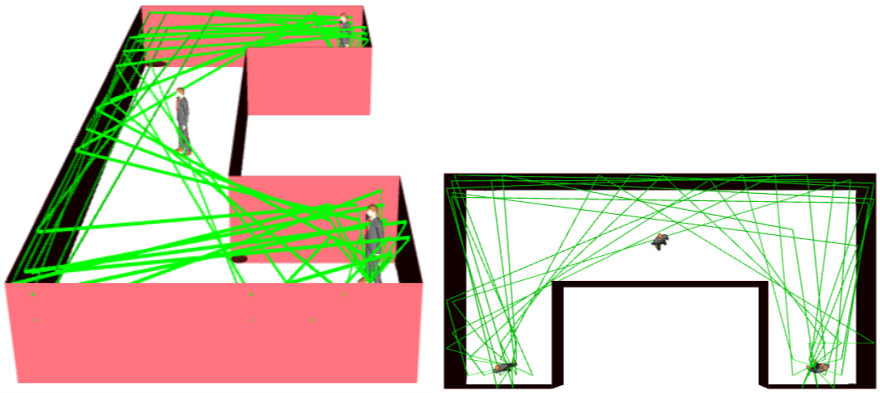

Figure 12: HyperSurface-controlled propagation, side and top views. Propagated waves avoid the eavesdropper by remaining confined at the highest parts of the floorplan.

antenna lobes towards the ceiling. COLLIMATE and STEER functions are applied to tiles, routing rays from the transmitter to the receiver. This is attained by first calculating the K tile-disjoint paths from the transmitter to the receiver, and then deploying STEER functions accordingly. The first impact tiles are configured to additionally collimate impinging waves as described. The performance and security benefits of the programmable wireless environment as summarized in Table 6. In the plain setup, the intended user receives -83 dBm total power, i.e., a total path loss of 53 dB. Moreover, the eavesdropper has better reception quality than the intended receiver, since he is physically closer to the transmitter. In the programmable environment case, the eavesdropping is completely mitigated, since the EM propagation remains confined to the upper part of the floorplan. Moreover, the intended recipient has a considerably better reception of $-47\,dBm$, i.e., a 36 dB improvement over the plain case.

Table 6: Comparison of total received/eavesdropped power, without 'phase_alter'.

	Received Power ($dBmW$)	
	HSF setup (Fig. 12)	Plain setup (Fig. 11)
User 1	-47	-83
User 2 (eavesdropper)	$-\infty$	-76

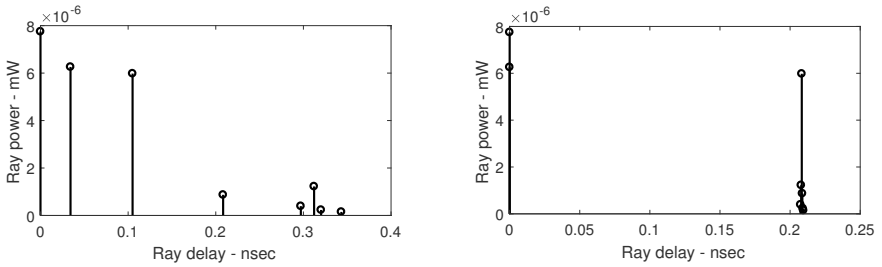

(a) Without 'PHASE_ALTER', received power $-76\,dBm$.

(b) With 'PHASE_ALTER', received power $-82.7\,dBm$.

Figure 13: Power Delay Profile for user 2 under natural propagation (Fig. 11), without and with 'PHASE_ALTER'.

Finally, we proceed to evaluate the phase control-based approach for eavesdropping mitigation. To this end, we return to the plain propagation shown in Fig. 11, i.e., no STEER or COLLIMATE functions are applied. Instead PHASE_ALTER functions are exclusively applied, to achieve the effect described in the context of Fig. 5.

Figure 13a shows the power-delay profile of the eavesdropper in the plain case. The x-axis is the timing of each received ray relative to the earlier ray, modulo the carrier period (i.e., multiplication of the x-axis values by $2\pi f$ return the relative phase in radians). The phase control-based mitigation pertains to altering the phase of each ray in a manner that cancels them out. In the case of Fig. 13a, the second and third rays are carry almost the same power and, therefore, they can be moved to opposite phases to cancel each other out. Rays four to eight can be synchronized and be opposed to the first and strongest ray. The described effects are shown in Fig. 13b.

The described phase control offers almost $6\,dB$ of extra signal attenuation at the eavesdropper. The maximal gains of this approach is strongly depended on the original power delay profile. The effects are expected to be optimal when there exist group rays that carry approximately the same power. Such groups can be subsequently phase-controlled to cancel each other out. Finally, it is noted that phase control is naturally expected to be sensitive to errors, such as the perceived location of users. Adaptive control loops are expected to be required in order to achieve the eavesdropping mitigation gains. Moreover, the phase control approach may only be used as a last resort, i.e., when the

ray-routing approach cannot offer routes that avoid the potential eavesdropper.

7.3. Discussion and Research Directions

The results of Section 7 demonstrated the performance and security potential of the proposed softwarization of wireless indoor environments.

In terms of performance objectives, the evaluation showcased path loss and multi-path fading mitigation. Even at the highly-challenging $60\,GHz$ communications, a HyperSurface tile-coated indoor setup exhibited significant improvements in received power levels and delay spread. Such traits can benefit the communication distance of devices and their energy consumption, without dissipating more energy in the–already EM-strained–environments via retransmitters. In terms of security, HyperSurfaces are shown to be promising enforcers of Physical Layer Security, due to their ability to micro-manage EM waves. Strong protection against eavesdropping can be attained by routing waves via improbable paths, avoiding potential eavesdropper altogether, or by ensuring coherent reception only near the receiver.

These promising traits can encourage further exploration of the HyperSurface concept in additional usage domains. Multiple applications can be studied in both indoor and outdoor environments, and in the context of multiple systems, such as 5G, IoT and D2D, where security, ultra-low latency, high bandwidth, and support for massive numbers of devices are important [3]. Moreover, HyperSurfaces may act as an enabler for upcoming THz communications. Operation in this band promises exceptional data rates and hardware size minimization at the nano-level, which can enable a wide range of groundbreaking applications [55]. Nonetheless, the THz band is susceptible to acute signal attenuation owed to molecular absorption. HyperSurfaces with graphene-based meta-atom designs could act as a smart environment for up to $1.8\,THz$ communications [56], mitigating the attenuation effects and extending the communication range.

Further research directions can also study the placement and topology of tiles within an environment, as well as their networking aspects. Partial, optimized coverage of an environment may provide sufficient performance gains over a full deployment. Coverage versus gains studies can quantify this aspect. Moreover, the networking topology, e.g., comprising a hierarchy of environment controllers and their corresponding sets of tiles is subject to optimization, in order to achieve a timely EM wave sensing and environment re-configuration loop. Communication protocols between tiles and controllers is similarly subject to optimization.

Finally, wireless power transfer is another promising application, apart from wireless performance and security. The ability of HyperSurfaces to collimate, steer and focus EM waves can be employed to transfer and charge devices wirelessly over long distances.

8. Conclusion

In this paper we proposed an indoor wireless communication paradigm where the electromagnetic propagation environment becomes aware of the ongoing communications within it.The key idea is to coat objects such as walls, doors and furniture with HyperSurface tiles, a forthcoming type of material with programmable electromagnetic behavior. HyperSurfaces can exert fine-grained control over impinging electromagnetic waves, steering them toward completely custom directions, polarizing them or fully absorbing them. HyperSurfaces have inter-networking capabilities, allowing for the first time the participation of electromagnetic properties of materials into control loops. A central server maintains a view of the communicating devices within an indoor space, and subsequently sets the tile electromagnetic configuration in accordance with any optimization objective. The HyperSurface tile concept has been evaluated in 2.4 and $60\,GHz$ setups, which demonstrated its high potential for path loss and multi-path fading mitigation, from microwave to mm-wave setups. Moreover, HyperSurfaces were shown to be efficient enforcers of physical layer security, micromanaging the propagation of electromagnetic waves in novel, eavesdropping-blocking ways.

Acknowledgment

This work was partially funded by the European Union via the Horizon 2020: Future Emerging Topics call (FETOPEN), grant EU736876, project VISORSURF (http://www.visorsurf.eu).

[1] Z. Pi, J. Choi, and R. Heath, "Millimeter-wave gigabit broadband evolution toward 5G: fixed access and backhaul," *IEEE Communications Magazine*, vol. 54, no. 4, pp. 138–144, 2016.

[2] T. Yilmaz and O. B. Akan, "Millimetre-Wave Communications for 5G Wireless Networks," *Opportunities in 5G Networks: A Research and Development Perspective*, pp. 425–440, 2016.

[3] A. Aijaz, M. Simsek, M. Dohler, and G. Fettweis, "Shaping 5G for the Tactile Internet," in *5G Mobile Comm.*, pp. 677–691, Springer, 2017.

[4] J.-M. Kelif *et al.*, "A 3D beamforming analytical model for 5G wireless networks," in *14th WiOpt*, pp. 1–8, 2016.

[5] S. V. Hum, M. Okoniewski, and R. J. Davies, "Modeling and design of electronically tunable reflectarrays," *IEEE transactions on Antennas and Propagation*, vol. 55, no. 8, pp. 2200–2210, 2007.

[6] J. Huang, L. I. Wenxiang, Y. Su, and F. Wang, "Multi-rate combination of partial information based routing and adaptive modulation and coding for space deterministic delay/disruption tolerant networks," *IET Communications*, 2017.

[7] S. Han and K. G. Shin, "Enhancing Wireless Performance Using Reflectors," in *INFOCOM 2017*, pp. 1–10.

[8] Y. Chen, S. He, F. Hou, Z. Shi, and J. Chen, "Promoting device-to-device communication in cellular networks by contract-based incentive mechanisms," *IEEE Network*, vol. 31, no. 3, pp. 14–20, 2017.

[9] A. Y. Zhu *et al.*, "Traditional and emerging materials for optical metasurfaces," *Nanophotonics*, vol. 6, no. 2, 2017.

[10] A. E. Minovich, A. E. Miroshnichenko, A. Y. Bykov, T. V. Murzina, D. N. Neshev, and Y. S. Kivshar, "Functional and nonlinear optical metasurfaces: Optical metasurfaces," *Laser & Photonics Reviews*, vol. 9, no. 2, pp. 195–213, 2015.

[11] S. Lucyszyn, *Advanced RF MEMS*. The Cambridge RF and microwave engineering series, NY: Cambridge Univ. Press, 2010.

[12] H.-T. Chen, A. J. Taylor, and N. Yu, "A review of metasurfaces: physics and applications," *Reports on progress in physics. Physical Society (Great Britain)*, vol. 79, no. 7, p. 076401, 2016.

[13] S. H. Lee *et al.*, "Switching terahertz waves with gate-controlled active graphene metamaterials," *Nature Materials*, vol. 11, no. 11, pp. 936–941, 2012.

[14] "Wi-fi home design."

[15] N. Yu, P. Genevet, M. A. Kats, F. Aieta, J.-P. Tetienne, F. Capasso, and Z. Gaburro, "Light propagation with phase discontinuities: generalized laws of reflection and refraction," *science*, p. 1210713, 2011.

[16] A. Welkie, L. Shangguan, J. Gummeson, W. Hu, and K. Jamieson, "Programmable radio environments for smart spaces," in *Proceedings of the 16th ACM Workshop on Hot Topics in Networks*, HotNets-XVI, (New York, NY, USA), pp. 36–42, ACM, 2017.

[17] C. Liaskos, A. Tsioliaridou, A. Pitsillides, I. F. Akyildiz, N. Kantartzis, A. Lalas, X. Dimitropoulos, S. Ioannidis, M. Kafesaki, and C. Soukoulis, "Design and Development of Software Defined Metamaterials for Nanonetworks," *IEEE Circuits and Systems Magazine*, vol. 15, no. 4, pp. 12–25, 2015.

[18] B. Banerjee, *An introduction to metamaterials and waves in composites*. Boca Raton, FL: CRC Press/Taylor & Francis Group, 2011.

[19] A. D. Wyner, "The wire-tap channel," *Bell system technical journal*, vol. 54, no. 8, pp. 1355–1387, 1975.

[20] M. Bloch, J. Barros, M. R. Rodrigues, and S. W. McLaughlin, "Wireless information-theoretic security," *IEEE Transactions on Information Theory*, vol. 54, no. 6, pp. 2515–2534, 2008.

[21] I. F. Akyildiz, S. Nie, S.-C. Lin, and M. Chandrasekaran, "5G roadmap: 10 key enabling technologies," *Computer Networks*, vol. 106, pp. 17–48, 2016.

[22] C. Wang and H. Wang, "Physical layer security in millimeter wave cellular networks," *IEEE Transactions on Wireless Communications*, vol. 15, pp. 5569–5585, Aug 2016.

[23] Y. Zhu, L. Wang, K. Wong, and R. W. Heath, "Physical layer security in large-scale millimeter wave ad hoc networks," in *2016 IEEE Global Communications Conference (GLOBECOM)*, pp. 1–6, Dec 2016.

[24] N. Yang, L. Wang, G. Geraci, M. Elkashlan, J. Yuan, and M. D. Renzo, "Safeguarding 5g wireless communication networks using physical layer security," *IEEE Communications Magazine*, vol. 53, pp. 20–27, April 2015.

[25] D. Kapetanovic, G. Zheng, and F. Rusek, "Physical layer security for massive mimo: An overview on passive eavesdropping and active attacks," *IEEE Communications Magazine*, vol. 53, pp. 21–27, June 2015.

[26] A. Garnaev, M. Baykal-Gursoy, and H. V. Poor, "Incorporating attack-type uncertainty into network protection," *IEEE Transactions on Information Forensics and Security*, vol. 9, no. 8, pp. 1278–1287, 2014.

[27] Y. Wu, R. Schober, D. W. K. Ng, C. Xiao, and G. Caire, "Secure massive mimo transmission with an active eavesdropper," *IEEE Transactions on Information Theory*, vol. 62, pp. 3880–3900, July 2016.

[28] X. Zhang and E. W. Knightly, "Pilot distortion attack and zero-startup-cost detection in massive mimo network: From analysis to experiments," *IEEE Transactions on Information Forensics and Security*, 2018.

[29] J. Zhu, R. Schober, and V. K. Bhargava, "Secure transmission in multicell massive mimo systems," *IEEE Transactions on Wireless Communications*, vol. 13, no. 9, pp. 4766–4781, 2014.

[30] M. Haus, M. Waqas, A. Y. Ding, Y. Li, S. Tarkoma, and J. Ott, "Security and privacy in device-to-device (d2d) communication: A review," *IEEE Communications Surveys Tutorials*, vol. 19, pp. 1054–1079, Secondquarter 2017.

[31] W. K. Harrison, J. Almeida, M. R. Bloch, S. W. McLaughlin, and J. Barros, "Coding for secrecy: An overview of error-control coding techniques for physical-layer security," *IEEE Signal Processing Magazine*, vol. 30, pp. 41–50, Sept 2013.

[32] H. V. Poor and R. F. Schaefer, "Wireless physical layer security," *Proceedings of the National Academy of Sciences*, vol. 114, no. 1, pp. 19–26, 2017.

[33] K. Iwaszczuk *et al.*, "Flexible metamaterial absorbers for stealth applications at terahertz frequencies," *Optics Express*, vol. 20, no. 1, p. 635, 2012.

[34] R. J. Mailloux, *Phased array antenna handbook*, vol. 2. Artech House Boston, 2005.

[35] H. Yang, X. Cao, F. Yang, J. Gao, S. Xu, M. Li, X. Chen, Y. Zhao, Y. Zheng, and S. Li, "A programmable metasurface with dynamic polarization, scattering and focusing control," *Scientific reports*, vol. 6, p. 35692, 2016.

[36] PCBcart, "Printed circuit board calculator," 2017.

[37] M. Caironi, *Large area and flexible electronics*. John Wiley & Sons, 2015.

[38] M. A. U. Karim, S. Chung, E. Alon, and V. Subramanian, "Fully inkjet-printed stress-tolerant microelectromechanical reed relays for large-area electronics," *Advanced Electronic Materials*, vol. 2, no. 5, 2016.

[39] R. Parashkov, E. Becker, T. Riedl, H.-H. Johannes, and W. Kowalsky, "Large area electronics using printing methods," *Proceedings of the IEEE*, vol. 93, no. 7, pp. 1321–1329, 2005.

[40] K. Wiesenhütter and W. Skorupa, "Low-cost and large-area electronics, roll-to-roll processing and beyond," in *Subsecond Annealing of Advanced Materials*, pp. 271–295, Springer International Publishing, 2014.

[41] "Printing cost calculator," May 2017.

[42] I. F. Akyildiz *et al.*, "Nanonetworks: A new communication paradigm," *Computer Networks*, vol. 52, no. 12, pp. 2260–2279, 2008.

[43] J. E. Hopcroft, R. Motwani, and J. D. Ullman, *Automata theory, languages, and computation*, vol. 24. 2006.

[44] C. Verikoukis *et al.*, "Internet of Things: Part 2," *IEEE Communications Magazine*, vol. 55, no. 2, pp. 114–115, 2017.

[45] C. L. Holloway *et al.*, "An Overview of the Theory and Applications of Metasurfaces: The Two-Dimensional Equivalents of Metamaterials," *IEEE Antennas and Propagation Magazine*, vol. 54, no. 2, pp. 10–35, 2012.

[46] T. Saeed *et al.*, "Fault adaptive routing in metasurface controller networks," in *Proceedings of the 11th International Workshop on Network on Chip Architectures (NoCArc'18)*, (Fukuoka, Japan), 2018.

[47] R. L. Haupt and D. H. Werner, *Genetic algorithms in electromagnetics*. John Wiley & Sons, 2007.

[48] A. Tsioliaridou, C. Liaskos, A. Pitsillides, and S. Ioannidis, "A novel protocol for network-controlled metasurfaces," in *ACM NANOCOM'17*, NanoCom '17, (New York, NY, USA), pp. 3:1–3:6, ACM, 2017.

[49] J. Chen *et al.*, "Pseudo lateration: Millimeter-wave localization using a single rf chain," in *Wireless Communications and Networking Conference (IEE WCNC)*, pp. 1–6, 2017.

[50] Actix Ltd, "Radiowave Propagation Simulator SE," *http://actix.com*, 2010.

[51] M. Yazdi and M. Albooyeh, "Analysis of Metasurfaces at Oblique Incidence," *IEEE Transactions on Antennas and Propagation*, vol. 65, no. 5, pp. 2397–2404, 2017.

[52] M. Albooyeh *et al.*, "Resonant metasurfaces at oblique incidence: interplay of order and disorder," *Scientific reports*, vol. 4, p. 4484, 2014.

[53] Mathworks, "Genetic algorithm: Finding global optima for highly nonlinear problems," 2017.

[54] S. Luke, *Essentials of metaheuristics*. [S.l.]: Lulu, 1 ed., 2009.

[55] I. F. Akyildiz, M. Pierobon, S. Balasubramaniam, and Y. Koucheryavy, "The internet of bio-nano things," *IEEE Communications Magazine*, vol. 53, no. 3, pp. 32–40, 2015.

[56] K. Fan *et al.*, "Optically Tunable Terahertz Metamaterials on Highly Flexible Substrates," *IEEE Transactions on Terahertz Science and Technology*, vol. 3, no. 6, pp. 702–708, 2013.

Christos Liaskos received the Diploma in Electrical and Computer Engineering from the Aristotle University of Thessaloniki (AUTH), Greece in 2004, the MSc degree in Medical Informatics in 2008 from the Medical School, AUTH and the PhD degree in Computer Networking from the Dept. of Informatics, AUTH in 2014. He has published work in several venues, such as IEEE Transactions on: Networking, Computers, Vehicular Technology, Broadcasting, Systems Man and Cybernetics, Networks and Service Management, Communications, INFOCOM. He is currently a researcher at the Foundation of Research and Technology, Hellas (FORTH). His research interests include computer networks, security and nanotechnology, with a focus on developing nanonetwork architectures and communication protocols for future applications.

Shuai Nie received the B.S. degree in Electrical Engineering from Xidian University in 2012, and the M.S. degree in Electrical Engineering from New York University in 2014. Currently, she is working toward the Ph.D. degree in electrical and computer engineering at the Georgia Institute of Technology under the supervision of Prof. Ian F. Akyildiz. Her research interests include terahertz band and millimeter-wave communication networks and the wireless communication system for 5G and beyond.

Ageliki Tsioliaridou received the Diploma and PhD degrees in Electrical and Computer Engineering from the Democritus University of Thrace (DUTH), Greece, in 2004 and 2010, respectively. Her research work is mainly on the field of Quality of Service in computer networks. Additionally, her recent research interests lie in the area of nanonetworks, with specific focus on architecture, protocols, security and authorization issues. She has contributed to a number of EU, ESA and National research projects. She is currently a researcher at the Foundation of Research and Technology, Hellas (FORTH).

Andreas Pitsillides is a Professor in the Department of Computer Science, University of Cyprus, heads NetRL, the Networks Research Laboratory he founded in 2002, and is appointed Visiting Professor at the University of the Witwatersrand (Wits), School of Electrical and Information engineering, Johannesburg, South Africa. Earlier (2014-2017) Andreas was appointed Visiting Professor at the University of Johannesburg, Department of Electrical and Electronic Engineering Science, South Africa. His broad research interests include communication networks (fixed and mobile/wireless), Nanonetworks and Software Defined Metasurfaces/Metamaterials, the Internet- and Web- of Things, Smart Spaces (Home, Grid, City), and Internet technologies and their application in Mobile e-Services, especially e-health, and security. He has a particular interest in adapting tools from various fields of applied mathematics such as adaptive non-linear control theory, computational intelligence, game theory, and recently complex systems and nature inspired techniques, to solve problems in communication networks. Published over 270 referred papers in flagship journals (e.g. IEEE, Elsevier, IFAC, Springer), international conferences and book chapters, 2 books (one edited), participated in over 30 European Commission and locally funded research projects as principal or co-principal investigator, received several awards, including best paper, presented keynotes, invited lectures at major research organisations, short courses at international conferences and short courses to industry, and serves/served on several journal and conference executive committees.

Sotiris Ioannidis received a BSc degree in Mathematics and an MSc degree in Computer Science from the University of Crete in 1994 and 1996 respectively. In 1998 he received an MSc degree in Computer Science from the University of Rochester and in 2005 he received his PhD from the University of Pennsylvania. Ioannidis held a Research Scholar position at the Stevens Institute of Technology until 2007, and since then he is Research Director at the Institute of Computer Science of the Foundation for Research and Technology - Hellas. Since November 2017 he is a member of the European Union Agency for Network and Information Security (ENISA) Permanent Stakeholders Group (PSG). His research interests are in the area of systems, networks, and security. Ioannidis has authored more than 100 publications in international conferences and journals, as well as book chapters, including ACM CCS, ACM/IEEE ToN, USENIX ATC, NDSS, and has both chaired and served in numerous program committees in prestigious international conferences. Ioannidis is a Marie-Curie Fellow and has participated in numerous international and European projects. He has coordinated a number of European and National projects (e.g. PASS, EU-INCOOP, GANDALF, SHARCS) and is currently the project coordinator of the THREAT-ARREST, I-BiDaaS, BIO-PHOENIX, IDEAL-CITIES, CYBERSURE, and CERTCOOP European projects.

Ian F. Akyildiz is currently the Ken Byers Chair Professor in Telecommunications with the School of Electrical and Computer Engineering, Director of the Broadband Wireless Networking Laboratory, and Chair of the Telecommunication Group at Georgia Institute of Technology, Atlanta, USA. Since 2011, he serves as a Consulting Chair Professor with the Department of Information Technology, King Abdulaziz University, Jeddah, Saudi Arabia, and with the Computer Science Department at the University of Cyprus since January 2017. He is a Megagrant Research Leader with the Institute for Information Transmission Problems at the Russian Academy of Sciences, in Moscow, Russia, since May 2018. His current research interests are in 5G wireless systems, nanonetworks, Terahertz band communications, and wireless sensor networks in challenged environments. He is an IEEE Fellow (1996) and an ACM Fellow (1997). He received numerous awards from the IEEE and the ACM, and many other organizations. His h-index is 115, and the total number of citations is above 105K as per Google scholar as of October 2018.